A Study of two phases heat transport capacity in a Micro Heat Pipe

Cheng-Hsing Hsu[1], Kuang-Yuan Kung[2,*], Shu-Yu Hu[1], and Ching-Chuan Chang[1]
[1]Department of Mechanical Engineering Chung-Yuan Christian University.
[2,*]Department of Mechanical Engineering Nanya Institute of Technology.

kykoung@nanya.edu.tw http://www.nanya.edu.tw/

Abstract: Present study modifies Cotter's model by using the dimensionless liquid flow shape factor, K_1, to predict the maximum heat transport capacity and to discus the effects of contact angle. The results indicated that as the dimensionless liquid flow shape factor, K_1 , decreases, the friction effects on the vapor-liquid interface flow, L_v , increases, and the liquid flow influenced by the vapor flow also increases. The predicted maximum heat transport capacity agrees well with Babin's experimental data of a copper-water micro heat pipe under, L_v =1 and contact angle, $\alpha = 10^o$. In a micro heat pipe, the results indicated that both the maximum heat transport capacity and K_1 increases with a increasing contact angle α .

Key-Words: Cotter's model, Contact angle, Heat pipe, Heat transport capacity,Shape factor, Dimensionless

1 Introduction

Heat pipes are widely used in related heat transfer application. Analyses of heat pipes, both numerical and experimental, have been performed by many investigators [1-15].

Due to the complexity of getting as analytical solution for heat pipe operation, some models without the effects of shearing stress on the liquid-vapor interface has been intensively study by [1-4]. The first analytical model for micro-heat pipe was presented by Cotter [1]. The capillary pressure gradient due to the variation of radius curvature was assumed to be the driving force of the liquid flow, zero liquid-vapor interface velocity, and laminar incompressible vapor flow region. Ha and Peterson [2] applied Xu [3] governing equation to modify Cotter model. They defined dimensionless shape factor and reported the effects of the contact angle of liquid vapor interface.

Ayyaswamy [4] analyzed a steady flow in a groove by Galerkin boundary method. He concluded that the effects of the contact angle of solid-liquid on the average velocity are minus under small groove tip angle. Babin et al [5] reported the experimental results of a 1mm heat pipe of Cotter's model by using water as working fluid in copper or silver.

Because it is important to know the effects of shearing stress on the liquid-vapor interface, many researches [6-12] have been depicted it. Ma et al. [6] investigated the effects of shearing force on the liquid-vapor interface inducing the pressure gradient in the fluid flow in a triangular groove. They concluded that the frictional factor Reynolds number is a function of groove tip angle, the contact angle of solid-vapor, and the liquid-vapor interface.

The results are presented theoretical and experimental consistency. One of the most important characteristics of micro heat pipe is the maximum heat transport capacity, which has been discussed by [7-12]. Faghri [10] theoretically and experimentally investigated both axially grooved heat pipes and flat miniature heat pipes. The maximum heat transfer capability in axially grooved heat pipes is subjected to the geometry of the heat pipes and the contact angle of liquid-solid interface.

The present paper deals with the numerical prediction of Micro heat pipes. It shows the volume flow rate, maximum heat transport capacity and input power of micro capillary grooves under the influence of the shearing stress of interface, contact angle and length. The numerical results are compared to the experimental data of Babin [1] and Ma et al. [6] model.

2 Theoretical Analysis

It is clearly that the vapor flow direction strongly impacts the flow velocity and behavior of liquid surface[5]. But the shearing stress on the liquid-vapor interface was neglect in Cotter's model [1], which results in a larger heat transfer than real situation. The fundamental assumptions are two dimensional Newtonian incompressible flow, fully developed laminar vapor flow and no slip condition on liquid-solid interface [6]. The momentum equation can be written as

$$\frac{1}{r}\frac{\partial}{\partial r}\left(r\frac{\partial u}{\partial r}\right)+\frac{1}{r^2}\frac{\partial^2 u}{\partial \theta^2}=\frac{1}{\mu}\frac{dp}{dz} \quad (1)$$

where u is axial velocity, z the corresponding axial coordinate, P the static pressure, μ the dynamic viscosity and θ groove angle. No slip conditions at the wall are assumed.

$$\theta = 0, \quad u = 0 \tag{2}$$

$$\theta = 2\phi, \quad u = 0 \tag{3}$$

In order to obtain a general solution, two boundary conditions in r direction are assumed. A trapezoid shape in liquid region is formed when $r = r_2$ ，the liquid surface velocity is defined as $\bar{u}_{r2}$ and zero liquid velocity at $r = r_1$. As $r_1 \to 0$, the solution relates to that obtained for a triangle groove, closed on these three sides.

Based on Ma et al. [6] dimensionless parameters as

$$u^* = \frac{u + \frac{r^2}{4\mu}\left(-dp/dz\right)}{\frac{r_1^2}{4\mu}\left(-dp/dz\right)} \tag{4}$$

$$x = \ln\frac{r}{r_1} \tag{5}$$

and ϕ is half-channel angle. The geometry on the interface of liquid-vapor depends major on the shape of the liquid flow passage with low Bond number conditions [6].They also describe radius as：

$$r_1 = r_{w1}\frac{\cos\phi}{\cos\left(\phi-\theta\right)} \tag{11}$$

$$r_2 = r_{w2} \times \frac{\cos\alpha\cos\left(\phi-\theta\right) - \left[\sin^2\phi - \cos^2\alpha\sin\left(\phi-\theta\right)\right]^{0.5}}{\cos\left(\alpha+\phi\right)} \tag{12}$$

Fourier transformation method and superposition is applied to the Laplace governing equation (6), where the exact solution is subjected to fit the boundary conditions given in equations (7)-(10).

The analytical velocity u can be shown as [6]

$$u = \left[\frac{r_1^2}{4\mu}\left(-dp/dz\right)\right] \times \left\{ \frac{2}{\pi}\sum_{n=1}^{\infty}\left[1-\left(-1\right)^n\right] \times \frac{1}{n} \times \frac{Hp \times \sinh\frac{n\pi}{2\phi}x + \sinh\frac{n\pi\left(a-x\right)}{2\phi}}{\sinh\frac{n\pi}{2\phi}a} \times \sin\frac{n\pi\theta}{2\phi} \right.$$
$$+ \frac{2}{\pi}\sum_{n=1}^{\infty}\frac{\left[1-(-1)^n\left(\frac{r_2}{r_1}\right)^2\right]\frac{1}{n}}{\left[1+\left(\frac{2a}{n\pi}\right)^2\right]} \times \frac{\sinh\frac{n\pi\theta}{a} + \sinh\frac{n\pi\left(2\phi-\theta\right)}{a}}{\sinh\frac{n\pi 2\phi}{a}} \times \sin\frac{n\pi}{a}x$$
$$\left. -\left(\frac{r}{r_1}\right)^2 \right\} \tag{13}$$

Where

The dimensionless governing equation and boundary conditions are

$$\frac{\partial^2 u^*}{\partial x^2} + \frac{\partial^2 u^*}{\partial \theta^2} = 0 \tag{6}$$

$$u^* = \left(\frac{r}{r_1}\right)^2 = e^{2x} \quad at \quad \theta = 0, \tag{7}$$

$$u^* = \left(\frac{r}{r_1}\right)^2 = e^{2x} \quad at \quad \theta = 2\phi, \tag{8}$$

$$u^* = 1 \quad at \quad x = 0, \tag{9}$$

$$u^* = \frac{\bar{u}_{r2} + \frac{r_2^2}{4\mu}\left(-dp/dz\right)}{\frac{r_1^2}{4\mu}\left(-dp/dz\right)} \quad at \quad x = \ln\left(\frac{r_2}{r_1}\right) \tag{10}$$

$$a = \ln\frac{r_2}{r_1} \tag{14}$$

$$Hp = \frac{\bar{u}_{r2} + \frac{r_2^2}{4\mu}\left(-dp/dz\right)}{\frac{r_1^2}{4\mu}\left(-dp/dz\right)} \tag{15}$$

and $\bar{u}_{r2}$ is the average velocity of liquid surface at $r = r_2$. This value depends on both the liquid and vapor flow characteristics and properties. Due to an irregular cross-section is shown due to the fractional interaction of liquid flow and vapor flow. It is quite difficult to get a general solution of the average velocity of liquid surface $\bar{u}_{r2}$. To avoid the rising difficulty of getting analytical solution, assume the liquid surface is free to the influence of frictional influences. The momentum equation can be written under these assumptions

$$\mu\frac{d^2u_f}{r^2 d\theta^2} = \frac{dp}{dz} \tag{16}$$

where u_f is the free liquid surface velocity without the effects of vapor shearing stress and the corresponding boundary conditions are:

$$u_f = 0 \quad at \quad \theta = 0 \tag{17}$$

$$u_f = 0 \quad at \quad \theta = 2\phi. \tag{18}$$

Integrating the momentum equation, the solution of equation (16) with these boundary conditions is:

$$u_f = \left(-\frac{1}{4\mu}\frac{dp}{dz}\right)\times \left\{\frac{r_{w2}\left\{\cos\alpha\cos(\phi-\theta)-\left[\sin^2\phi-\cos^2\alpha\sin\ (\phi-\theta)\right]^{0.5}\right\}}{\cos(\alpha+\phi)}\right\}^2 \times \left(4\phi\theta-2\theta^2\right) \tag{19}$$

The average velocity of the liquid flow is preferred in the actual situation, and it is written as:

$$\bar{u}_f = \frac{\int_0^{2\phi} u_f d\theta}{\int_0^{2\phi} d\theta} \tag{20}$$

Then the one dimensional average velocity of the free liquid surface can be obtained as:

$$\bar{u}_f = \frac{1}{2\phi}\int_0^{2\phi}\left(-\frac{1}{4\mu}\frac{dp}{dz}\right) \times\left\{\frac{r_{w2}\left\{\cos\alpha\cos(\phi-\theta)-\left[\sin^2\phi-\cos^2\alpha\sin(\phi-\theta)\right]^{0.5}\right\}}{\cos(\alpha+\phi)}\right\}^2 \times\left(4\phi\theta-2\theta^2\right)d\theta \tag{21}$$

Since the one dimensional assumption is insufficient for the actual case, a correction factor is necessary to modify it. This coefficient, K, can be determined experimentally. Utilizing the experimental data of Ayyaswamy et al.[4], Ma et al. [2] presented that the coefficient K, without notification, is simplified to be the value of 0.52 for a 60° channel angle. But the coefficient K should vary with the channel apex angle θ, by neglecting this effect Ma et al. [2] assumed the coefficient K to be a constant.

$$\bar{u}_f{}' = K\bar{u}_f \tag{22}$$

where $\bar{u}_f$ is defined in equation (21). Ma et al. [3]defined the actual velocity of the free liquid surface and a dimensionless liquid-vapor interface flow number L_v as:

$$L_v = \frac{\Delta\bar{u}}{\bar{u}_f{}'} \tag{23}$$

and

$$\Delta\bar{u} = \bar{u}_f{}' - \bar{u}_{r_2} \tag{24}$$

and $\bar{u}_f^{/}$ is the average velocity of the free liquid surface.

Ma et al [2] demonstrates L_v including the correction factor K which is from Ayyaswamy [4] experimental data. But correction factor K cannot show both of the effects on the liquid-vapor interface and liquid-solid interface. Ma et al. [2] define a dimensionless liquid-vapor interface flow number L_v subjected to the frictional impacts on the liquid-vapor interface.

The effects of shear stresses at the liquid surface are taken into consideration, which is due to frictional liquid-vapor interaction on the liquid flow. This paper is based upon Ma et al. [2] conclusion by adjusting L_v to study the impacts of the liquid-vapor interface on rheology.

The average velocity at r_2 is：

$$\bar{u}_{r_2} = \bar{u}_f{}'\left(1-L_v\right) \tag{25}$$

combine equations (21) and (25), $\bar{u}_{r_2}$ can be shown as：

$$\bar{u}_{r_2} = \frac{K(1-L_v)}{2\phi}\int_0^{2\phi}\left(-\frac{1}{4\mu}\frac{dp}{dz}\right) \times\left\{\frac{r_{w2}\left\{\cos\alpha\cos(\phi-\theta)-\left[\sin^2\phi-\cos^2\alpha\sin(\phi-\theta)\right]^{0.5}\right\}}{\cos(\alpha+\phi)}\right\}^2 \times\left(4\phi\theta-2\theta^2\right)d\theta \tag{26}$$

From the equation (26), the average velocity of the liquid surface is related to α, ϕ, θ, r_{w2}, dp/dz, K and L_v. The flow direction of the liquid and the vapor velocity is values of the dimensionless vapor flow number, L_v, which is well explained by Ma et al. [2].

In real situation, the value of L_v can be obtained by the method of Schlichting. The velocity distribution of the liquid fluid in a V groove at any position (r,θ) can be evaluated in equation (13), while the value of $\bar{u}_{r_2}$ is obtained. Furthermore, The volume flow rate, Q, through any crossection can be expressed as:

$$
\begin{aligned}
Q &= \int_0^{2\phi}\int_{r_1}^{r_2} urdrd\theta \\
&= \left[\frac{1}{4\mu}(-dp/dz)\right]\int_0^{2\phi} r_1^4 \\
&\left\{\sum_{n=1}^{\infty}\frac{2\cdot\left[1-(-1)^n\right]}{n\pi\cdot\sinh\left(\frac{n\pi}{2\phi}a\right)\cdot\left(1-\left(\frac{n\pi}{4\phi}\right)^2\right)}\left\{\left\{-\frac{1}{2}\sinh\left(\frac{n\pi}{2\phi}a\right)+\frac{n\pi}{8\phi}\left[\left(\frac{r_2}{r_1}\right)^2-\cosh\left(\frac{n\pi}{2\phi}a\right)\right]\right\}\right.\right. \\
&\qquad \left.\left.+Hp\left\{\frac{1}{2}\left(\frac{r_2}{r_1}\right)^2\sinh\left(\frac{n\pi}{2\phi}a\right)-\frac{n\pi}{8\phi}\left[\left(\frac{r_2}{r_1}\right)^2\cosh\left(\frac{n\pi}{2\phi}a\right)-1\right]\right\}\right\}\sin\frac{n\pi\theta}{2\phi}\right. \\
&\left.+\frac{1}{8a}\cdot\left(\frac{n\pi}{a}\right)^2\cdot\frac{\left[1-(-1)^n\left(\frac{r_2}{r_1}\right)^2\right]^2}{\left[1+\left(\frac{2a}{n\pi}\right)^2\right]^2}\times\frac{\sinh\frac{n\pi\theta}{a}+\sinh\frac{n\pi(2\phi-\theta)}{a}}{\sinh\frac{n\pi 2\phi}{a}}\right\}d\theta+ \\
&\left[\frac{1}{4\mu}(-dp/dz)\right]\int_0^{2\phi}\frac{r_1^4}{4}\left(1-\left(\frac{r_2}{r_1}\right)^4\right)d\theta
\end{aligned}
\tag{27}
$$

The parameters r_1, r_2, α and Hp in equation (27) are determined from equations (11), (12), (14) and (15), respectively.

Comparing Ma et al. [2] analysis, Cotter [1], by a dimensionless shape factor, K_1, presented the liquid mass flow rate as:

$$\dot{m}_l = -\frac{\mathrm{K}_1\rho_l A_l^2}{8\pi\mu}\frac{dp}{dz} \tag{28}$$

Where A_l is the liquid flow cross section area, ρ_l the liquid density and $\dot{m} = Q_t\rho_l$. Q_t is the liquid volume flow rate in heat pipe. Rearrange the above equation (28), K_1 may be obtained as

$$\mathrm{K}_1 = -\frac{8\pi\mu_l nQ}{A_l^2\left(\frac{dp}{dz}\right)} \tag{29}$$

n is the groove numbers of heat pipe, Q the volume flow rate.

The analytical velocity is gained by Fourier transform method and linear superposition to analysis the governing equation for a v-shape groove. By the momentum equation near the liquid-vapor interface to demonstrate the velocity near the interface, also define a dimensionless liquid-vapor interface flow number L_v to show the effect of shearing stress on the liquid velocity and to calculate the liquid volume flow rate.

Substitute the velocity distribution into Cotter's model and define a dimensionless liquid flow factor K_1 which shows the friction effects on liquid-vapor interface. These modify the maximum heat transfer in Cotter,s equation[1] and makes the numerical results more close to the Babin's experimental data[5].

3 Results and Discussion

The influence of shearing stress on liquid-vapor interface in a micro heat pipe is predicted. To verify the model predictions, results are compared with the experimental data reported by [1] and the numerical results by [9]. The frictional forces on the liquid-vapor interface could reduce the velocity of liquid flowing from condenser area toward evaporating area. Calculate the volume flow rate of liquid-wick in v-shape groove by analytical method and induce dimensionless parameter of flow factor L_v to inspect the frictional force effects on rheology. From equation (29), K_1 is proportional to volume flow rate Q, Q is related to the velocity scale and cross section area A_l, meanwhile the frictional force on the liquid interface induced by the reverse direction between vapor flow and liquid flow, thereafter reduced the liquid velocity.

Operating temperature lies in $40^o c - 70^o C$ in Babin et al[5], and the contact angle on the solid-liquid interface are in $10^o c - 50^o C$. Perterson and Ma [8] presents the dimensionless vapor-liquid interface flow number as L_v =0; 0.5; 1; 1.5. According to Babin[5] experimental data for a square heat pipe, the calculated result of Ha and Perterson [9] reports that the value of K_v =0.94, β =1.1343 and L_e =12.7mm, L_a =31.6mm , L_c =12.7mm.

This research tries to investigate the effects of shearing stress on liquid-vapor interface. Fig.1 presents the relationship between a dimensionless liquid flow factor K_1 and the contact angle of solid-liquid interface L_v, the K_1 changes along with the L_v value. It shows that the reverse steam flowing do have the frictional influences. And it also demonstrated that K_1 increases along with the increasing contact angle of solid - fluid. Babin[5] obviously neglects the influence of contact angle by fixed value of K_1 =0.6 and Cotter[1] simply put K_1=0.5. Use the analytical method in present study under the condition L_v =0 with contact angle of 10^0, and the value of K_1 is 0.31, which is less than Cotter's prediction.

Fig. 2 shows the variation of K_1 with the solid liquid contact angle α in a square groove for different values of L_v. It is observed that the lower value of K_1 will shown as increasing value of L_v under same contact angle α. Since the flow direction of vapor is reversed to the flow direction of liquid, it tends to induce a frictional force on the liquid-vapor interface, and the effects of vapor flow reducing the liquid flow by friction on interface is shown.

It is also shows that the value of K_1 increase with the increasing value of contact angle α .The physical dimensions of the triangular heat pipe are chosen as: $L_e = L_a = L_c = 5mm$, $\beta = 1.433$, K_v =0.86. By using the analytical method in present study, one can get the values of K_1. The K_1 involves a correction factor comparing to the K_1 in Ma et al. [10] researches, which is directly derived from Xu[3]. Ma et al. [10] defines K_1 as

$$\mathrm{K}_1 = \frac{4\pi c}{\kappa\beta^4} \tag{30}$$

where

$$c = 4c_1^3 \tan^2 \phi,$$

$$c_1 = \frac{1}{\tan\phi} + \phi - \frac{\pi}{2},$$

$$\beta = \sqrt{nc_1} \tag{31}$$

The dimensionless liquid flow shape factor, K_1,is calculated to be $K_1 = 0.135$ by Ma et al.[6, 9], using the parameter K induced by the influence on the solid-liquid contact angle without the impacts of the shearing stress on liquid-vapor interface. Under the condition of $\alpha = 10^o$; $L_v = 0$, (i.e. without the impacts of the shearing stress on liquid-vapor interface),we can get the value $K_1 = 0.191$, which is lower than Cotter's predicted K_1 value.

The maximum heat transport capacity is impacted by the values of K_1 . The maximum heat transport capacity presents a similar tendency between Cotter's prediction [1] and Babin's[5] experimental data, which is only half the values of Cotter's prediction.

Fig.3 to Fig.6 show the relationship between the operational temperature and the maximum heat transfer rate when the round heat pipe is ψ= 30^o . The contact angles (α) are respectively 10^o , 20^o , 30^o and 40^o . With changing of the operational temperature (T), the impacts of different L_v on the maximum heat transfer rate are compared. From these daigrams we learn that when L_v becomes greater, the maximum heat transfer rate will decrease. Thereby we find that the friction shear stress of air flow and fluid flow wil lower the maximum heat transfer rate.

Fig.7 to Fig.10 show the relationship between the operational temperature and the maximum heat transfer rate when the round heat pipe is ψ= 30^o . The number of flow of the dimensionless liquid-air contact surface is respectively L_v =0, L_v =0.5, L_v =1 and L_v =1.5. With changing of the operational temperature (T), the values of the maximum heat transfer rate at different contact angles (α) are compared. From observing these daigrams we learn that the higher the contact angle, the greater the maximum heat transfer rate.

Fig.11 to Fig.16 show the relationship between the operational temperature and the maximum heat transfer rate when the round heat pipe is ψ= 30^o . Respectively the operational temperatures are 40^o , 45^o , 50^o , 55^o , 60^o and 65^o . With changing of the contact angles (α), the values of the maximum heat transfer rate at different operational temperature (T) are compared. From these daigrams we can tell that the higher the operational temperature, the greater the maximum heat transfer rate.

Comparing the outcomes above with Babin experiment and Cotter prediction, we can see that as the contact angles (α) increases, the thermal performance is enhanced; that as number of flow of the dimensionless liquid-air contact surface L_v increases, the thermal performance will be compromised; that as the operational temperature (T) rises, the thermal performance will be improved.

Fig.17 presents the relationship between the operation temperature and the maximum heat transport capacity for a square micro heat pipe under different values of L_v . The contact angle of solid-liquid interface is 10^o , The results presents comparison of the maximum heat capacity with the numerical results given by Cotter and the experimental results given by Babin[5]. Fig.17 shows the maximum heat capacity increase with increasing value of the contact angle of the solid-liquid interface, but it decreased with higher values of L_v . The shearing stress induced by the friction force on the liquid-vapor interface will reduce the maximum heat transport capacity. In other word, the reverse direction between the flow direction of liquid and vapor will hinder the maximum heat transport capacity of the heat pipe.

Fig.18 to Fig.20 show the relationship between the included angle (ψ) of the trough opening and the maximum heat transfer rate when the operational temperature of the round heat pipe is T= 40^o . The contact angles (α) are respectively 20^o , 30^o and 40^o .

Fig.21 to Fig.26 show the relationship between the included angle (ψ) of the trough opening and the maximum heat transfer rate when the contact angles of the round heat pipe is α=10^o. Respectively the operational temperatures are 40^o, 45^o, 50^o, 55^o, 60^o and 65^o.

Fig.27 to Fig.29 presents the relationship between the operation temperature and the maximum heat transport capacity for a square micro heat pipe under different values of the contact angle on solid-liquid interface with L_v =0; 0.5; 1 ;1.5. It shows the maximum heat capacity increase with increasing value of the contact angle of the solid-liquid interface. The maximum heat transport capacity is coincide with the experimental results of Babin [5] underv $L_v = 1.5$ 、 $\alpha = 10^o$, and the same result of the onset of dryout is presented as the experimental data of Babin[5] under $\alpha = 20^o$. For circular heat pipe when ψ=13^o (groove angle 26^o) may obtain the biggest thermal properties.

4 Conclusion

A mathematical model in square grooves with vapor flow crossing the liquid-vapor interface in micro-heat pipes is developed [10]. Under the same contact angle of liquid-solid interface and groove angle, the maximum heat transfer rate and K_1 will decrease with increasing values of L_v.

The fractional force on the liquid-vpor interface will slow down the liquid velocity and lower the maximum heat transfer rate and the values of K_1. Under the same dimensionless parameter of liquid-solid interface L_v and groove angle, the maximum heat transfer rate and K_1 will increase with increasing values of contact angle α.

Acknowledgement:

The present investigation was supported by National Science Council of Taiwan under granted NSC-97-2221-E-253-014-

References:

[1] Cotter, T. P., Proceedings and Prospects of the Micro Heat Pipe, *Proceedings the 5th International Heat Pipe Conference*, Tsukuba, Japan. 1984, pp. 328-335.

[2] Ha, J. M. and Peterson, G. P., The Heat Transport Capacity of Micro Heat Pipes, *Transaction of ASME Journal of Heat Transfer*, Vol. 120, 1998, pp. 1064-1071.

[3] Xu, X., and Carey, V. P., Film Evaporation Form a Micro-Grooved Surface-An Approximate Heat Transfer Model and Its Comparison with Experimental Data, *AIAA J. of Thermophysics and Heat Transfer,* Vol.4, No.4, 1990, pp. 512-520.

[4] Ayyaswamy, P. S. , Catton, I. and Edwards, D.K., Capillary flow in triangular grooves, *ASME J*, Vol.41, 1974, pp.332-336.

[5] Babin, B.R., Peterson, G. P., and Wu, D., Steady-Sate Modeling and Testing of a Micro Heat Pipe, *ASME Journal of Heat Transfer,*Vol.112, 1990, pp.595-601.

[6] Ma, H. B., Peterson, G. P. and Lu, X. J., The Influence of Vapor-Liquid Interactions on the Liquid Pressure Drop in Triangular Microgrooves, *Int. J. Heat mass Transfer*, Vol. 37, No.15, 1994, pp. 2211-2219.

[7] Khrustalev, D., Faghri, A., Thermal analysis of a micro heat pipe, *ASME Journal of heat transfer,* Vol.116, 1994, pp. 189-198.

[8] Ma, H. B., Peterson, G. P., Theoretical Analysis of the Maximum Heat Transport in Triangular Grooves - a Study of Idealized Micro Heat Pipe, *ASME Journal of Heat Transfer*, Vol.118, 1996, pp. 731-739.

[9] Ma, H. B., Peterson, G. P., Experiment Investigation of the Maximum Heat Transport in Triangular Groove, *ASME Journal of Transactions,* Vol.118, 1996, pp. 740-746.

[10] Khrustalev. D., Faghri. A., Thermal Characteristics of Conventional and Flat Miniature Axially Grooved Heat Pipe, *ASME Journal of Transaction,* Vol.117, 1995, pp. 1048-1053.

[11] J. Van Beal and E. Peeters, Evaluation of the first micro combined heat and power for social housing Belgium, *Proceedings of the 6th WSEAS International Conference on Power Systems*, 2006.

[12] Kung, K.Y., Hsu, Cheng Hsing and Kuo, G.C., A study of liquid-vapor interface interaction effects in a micro heat pipe *WSEAS Transactions on Mathematics*, Vol.5, No.8, 2006, pp. 978-983.

[13] Nerg, Janne, Thermal analysis of a high-speed solid-rotor induction motor with a slitted solid-rotor, *WSEAS Transactions on Circuits and Systems*, Vol.5, No.3, 2006, pp.311-318.

[14] Attar, S. Sharifian, Yagoub, M.C.E., Mohammadi, F., Simulation of electro-thermal effects in device and circuit, *WSEAS Transactions on Circuits and Systems*, Vol.5, No.7, 2006, pp. 926-930.

[15] Fraguela, Andrés, Infante, Juan-Antonio, Ramos, Ángel Manuel, Rey, José María, Identification of a heat transfer coefficient when it is a function depending on temperature, *WSEAS Transactions on Mathematics*, Vol.7, No.4, 2008, pp. 160-172.

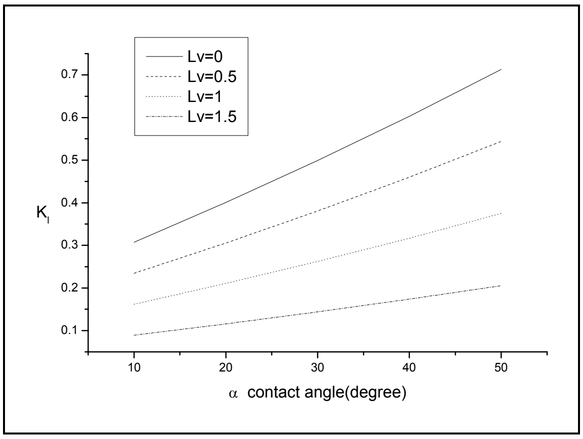

Fig.1 Dependence of K_1 on the contact angle α for various L_v with Square shape heat pipe.

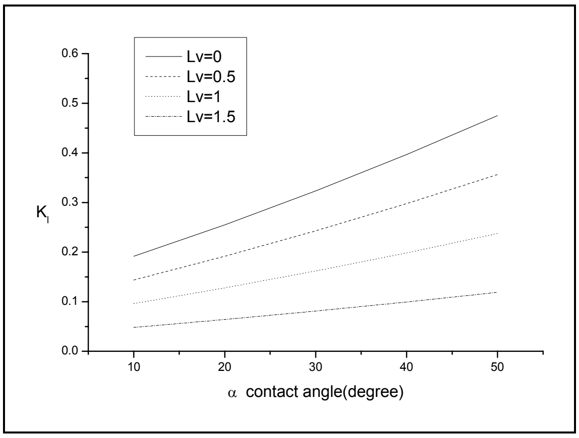

Fig. 2 Dependence of K_1 on the contact angle α for various L_v with equilateral triangle heat pipe.

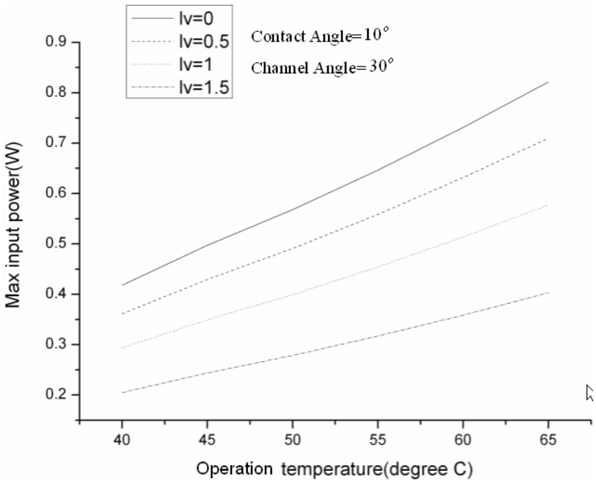

Fig. 3 The maximum heat transport capacity versus operation temperature for various L_V and α=10^o.

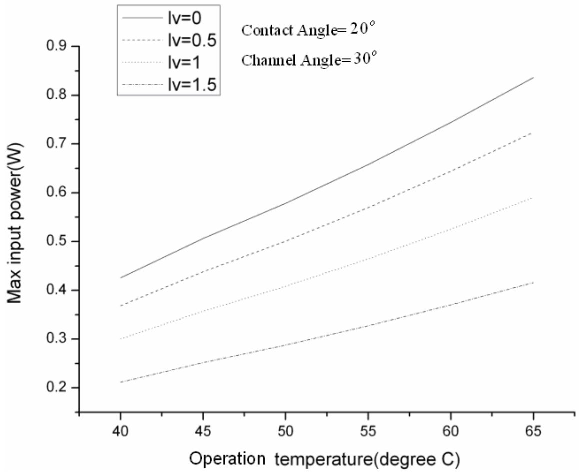

Fig. 4 The maximum heat transport capacity versus operation temperature for various L_V and α=20^o.

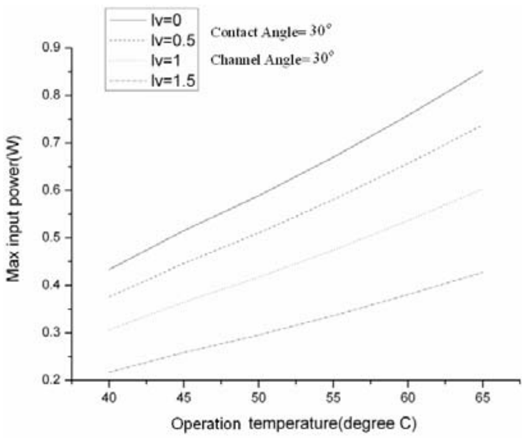

Fig. 5 The maximum heat transport capacity versus operation temperature for various L_V and α=30^o.

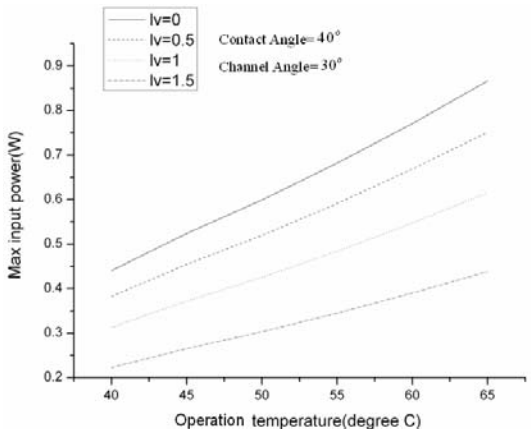

Fig. 6 The maximum heat transport capacity versus operation temperature for various L_V and α= 40^o.

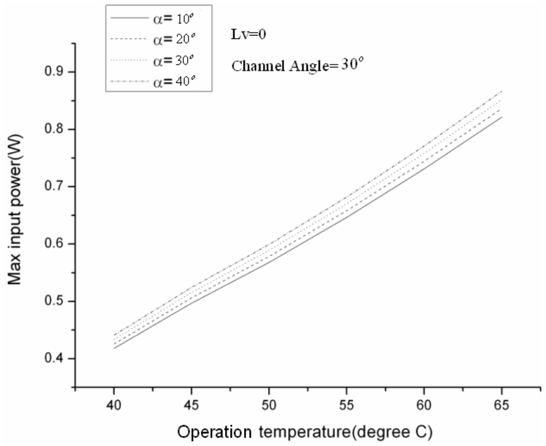

Fig. 7 The maximum heat transport capacity versus operation temperature for various α and L_V =0 .

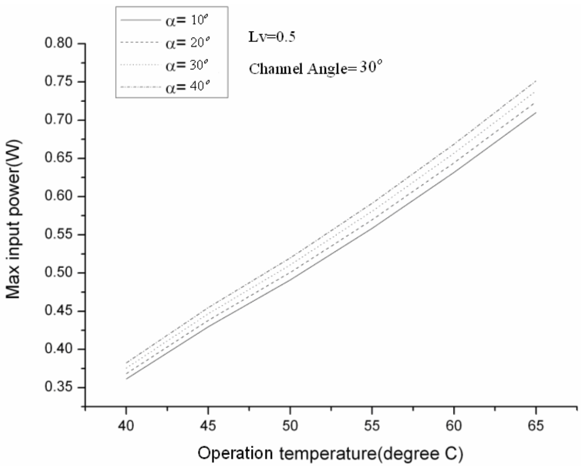

Fig. 8 The maximum heat transport capacity versus operation temperature for various α and L_V =0.5 .

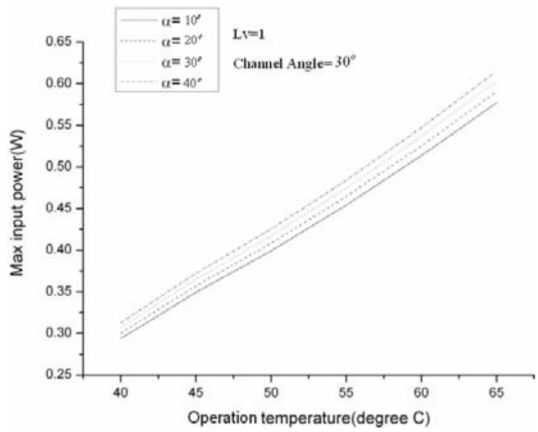

Fig.9 The maximum heat transport capacity versus operation temperature for various α and L_V =1 .

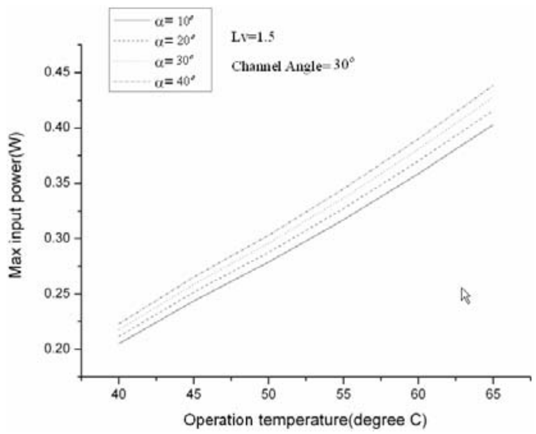

Fig. 10 The maximum heat transport capacity versus operation temperature for various α and L_V =1.5 .

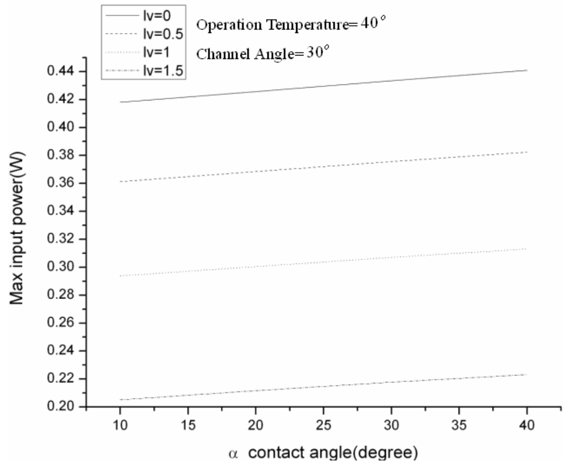

Fig. 11 The maximum heat transport capacity versus contact angle for various L_V and T= 40^o.

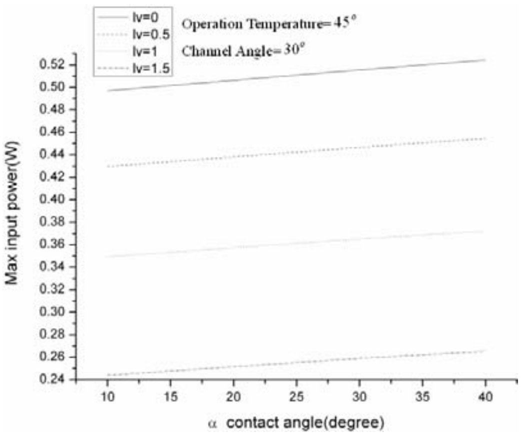

Fig. 12 The maximum heat transport capacity versus contact angle for various L_V and T= 45^o.

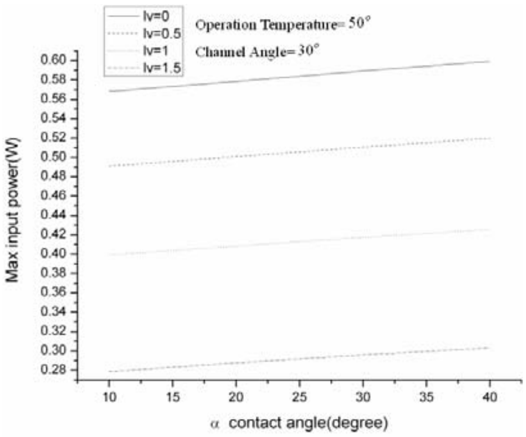

Fig. 13 The maximum heat transport capacity versus contact angle for various L_V and T= 50^o.

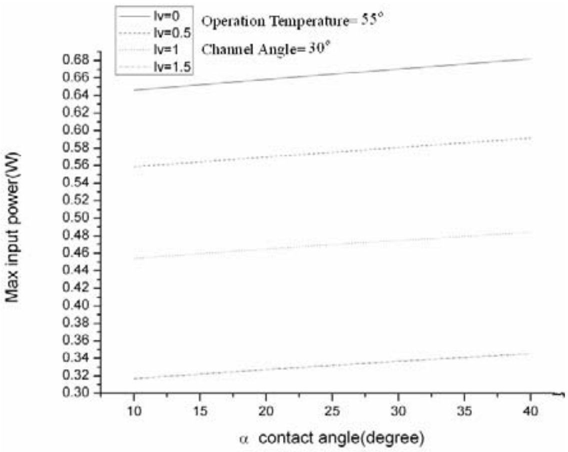

Fig. 14 The maximum heat transport capacity versus contact angle for various L_V and T= 55^o.

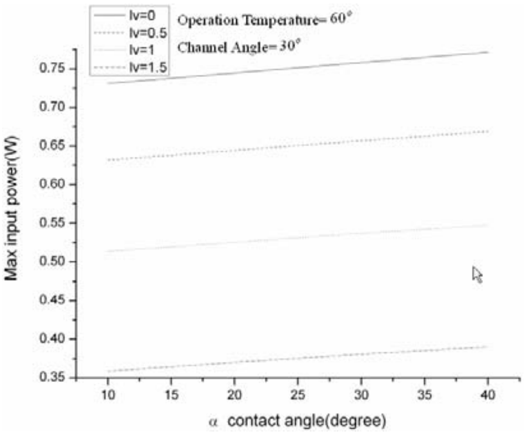

Fig. 15 The maximum heat transport capacity versus contact angle for various L_V and T= 60^o.

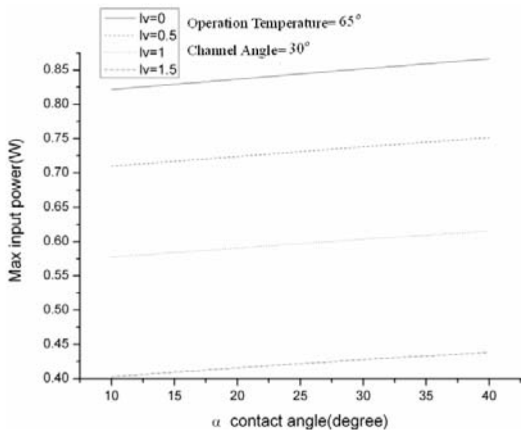

Fig. 16 The maximum heat transport capacity versus contact angle for various L_V and T= 65^o.

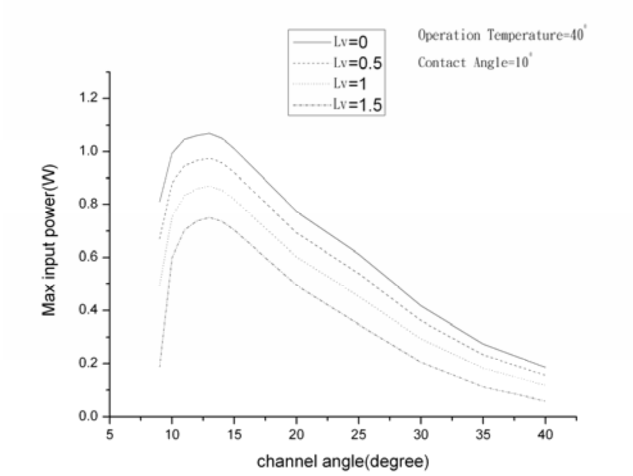

Fig. 17 The maximum heat transport capacity versus channel angle for various L_v and $\alpha = 10^o$.

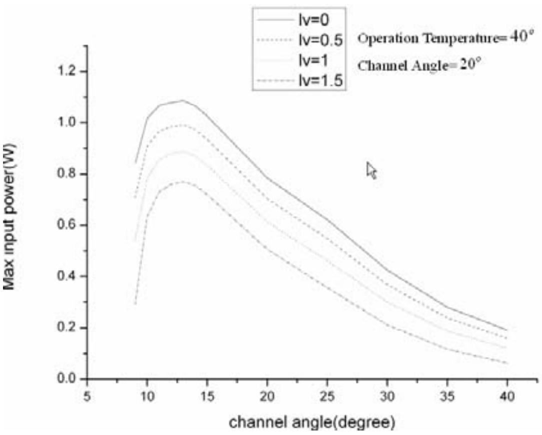

Fig. 18 The maximum heat transport capacity versus channel angle for various L_V and $\alpha = 20^o$.

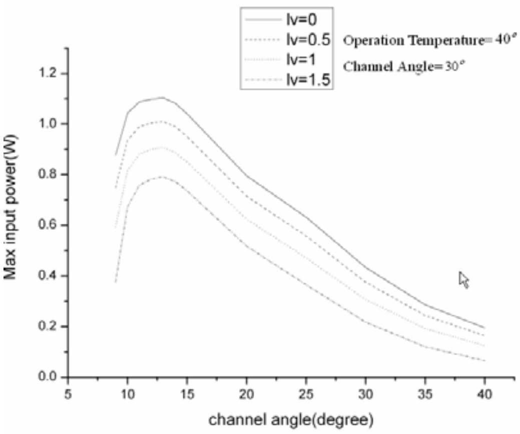

Fig. 19 The maximum heat transport capacity versus channel angle for various L_V and $\alpha = 30^o$.

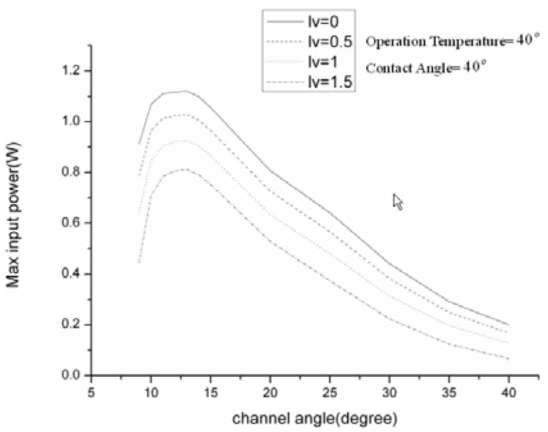

Fig. 20 The maximum heat transport capacity versus channel angle for various L_V and $\alpha = 40^o$.

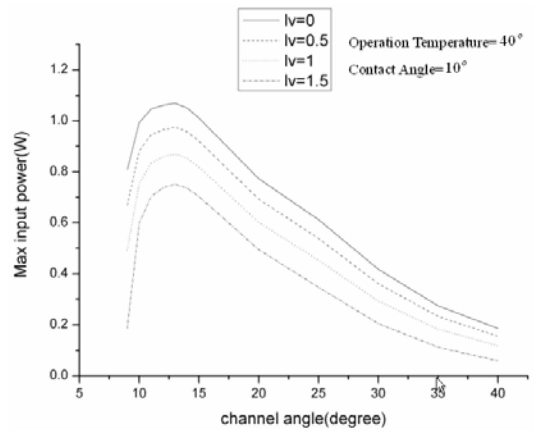

Fig. 21 The maximum heat transport capacity versus channel angle for various L_V and $T = 40^o$.

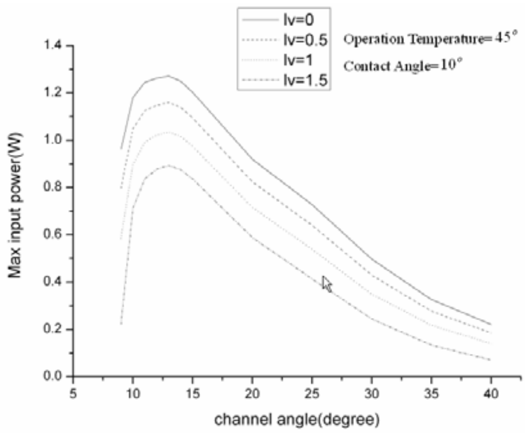

Fig. 22 The maximum heat transport capacity versus channel angle for various L_V and $T = 45^o$.

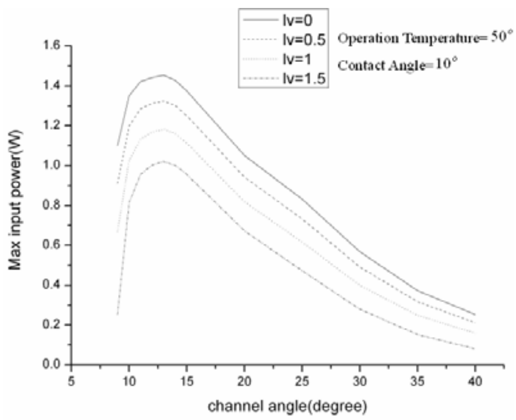

Fig. 23 The maximum heat transport capacity versus channel angle for various L_V and $T = 50^o$.

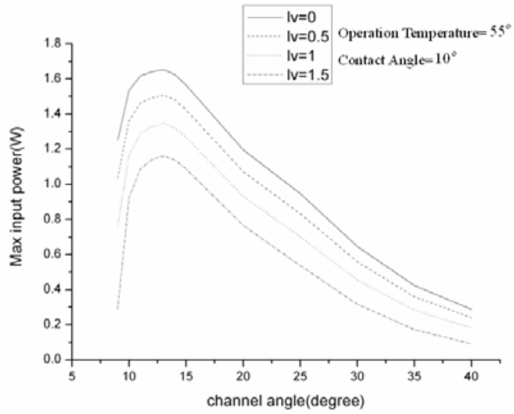

Fig. 24 The maximum heat transport capacity versus channel angle for various L_V and T= 55^o .

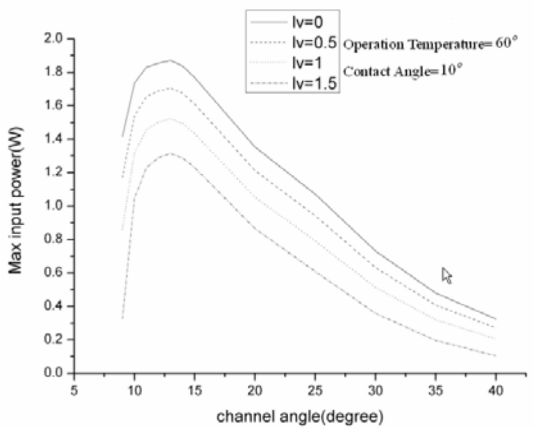

Fig. 25 The maximum heat transport capacity versus channel angle for various L_V and T= 60^o .

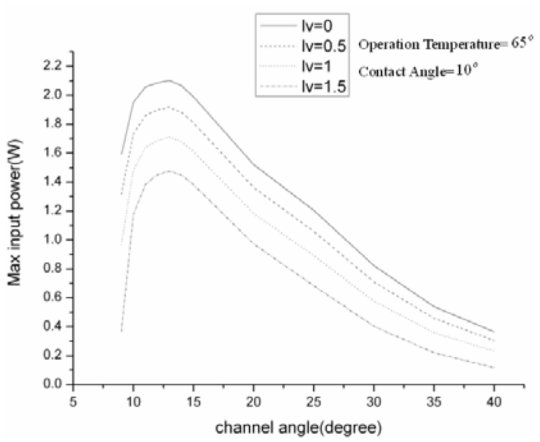

Fig. 26 The maximum heat transport capacity versus channel angle for various L_V and T= 65^o .

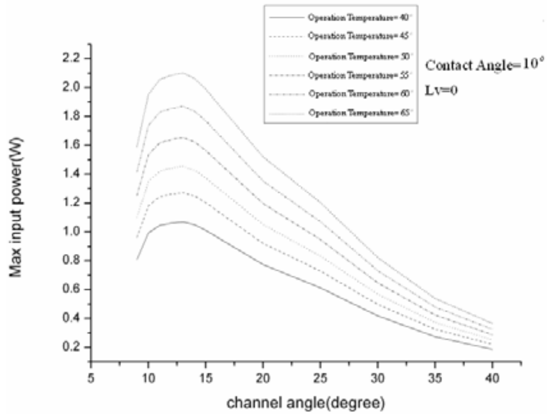

Fig. 27 The maximum heat transport capacity versus channel angle for various T and L_V =0 .

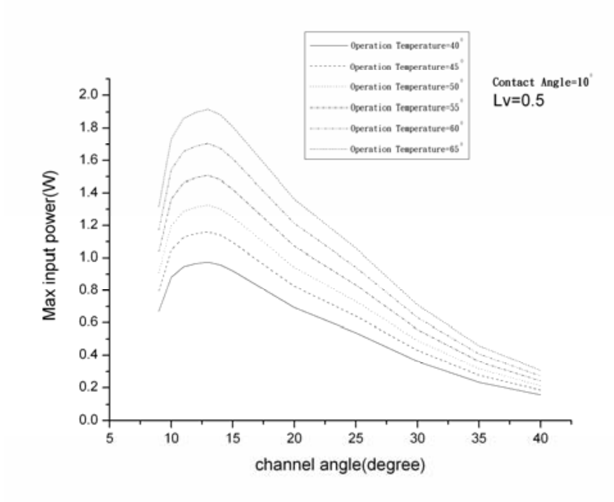

Fig.28 The maximum heat transport capacity versus channel angle for various operation temperature T and L_V =0.5 .

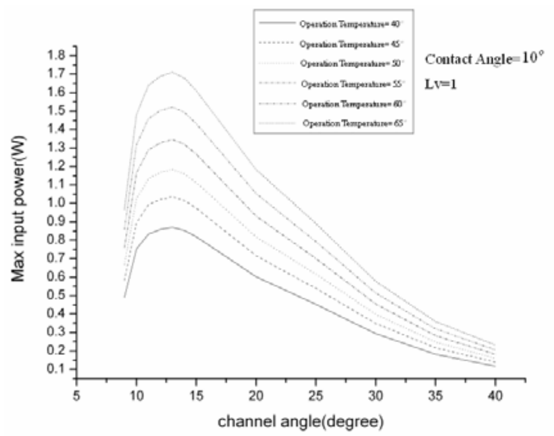

Fig. 29 The maximum heat transport capacity versus channel angle for various T and L_V =1 .